Mon. Not. R. Astron. Soc. **291,** 261–278 (1997)

Studies of ultracompact H II regions – I. Methanol maser survey of *IRAS*-selected sources

A. J. Walsh,[1] A. R. Hyland,[2] G. Robinson[3] and M. G. Burton[1]

[1]*Department of Astrophysics and Optics, School of Physics, University of New South Wales, NSW 2052, Australia*
[2]*Southern Cross University, Lismore, NSW 2480, Australia*
[3]*School of Physics, University College, University of New South Wales, Canberra, ACT, 2600, Australia*

Accepted 1997 April 27. Received 1997 April 7; in original form 1996 September 30

ABSTRACT

A survey of ultracompact (UC) H II regions has been carried out by searching for 6.669-GHz methanol maser emission from a sample of 535 *IRAS*-selected candidates. A total of 201 candidates exhibit methanol emission. These sources have been used, in conjunction with previously identified UC H II regions, to provide a base for further studies of such regions. Estimates of distances have indicated that the identified UC H II regions tend to have some Galactic structure but it is not clear whether they lie in or between the spiral arms of the Galaxy. The regions are tightly constrained to the plane of the Galaxy. Comparison of identified regions and *IRAS* sources selected by Wood & Churchwell indicates that there there is some degree of contamination, which could be due to an older phase in the life on an UC H II region where methanol maser emission is not apparent. Luminosities and spectral types have been derived for many of the regions. The maximum number of maser spots observed seems to increase with increasing peak maser luminosity, which indicates that the maser emission is more dependent on the abundance of methanol than the availability of far-infrared radiation.

Key words: surveys – stars: formation – H II regions – ISM: molecules – radio lines: ISM.

1 INTRODUCTION

An ultracompact (UC) H II region is a small, ionized bubble around an embedded massive (O or early B type) star. As well as being compact, the UC H II regions are characterized by having high emission measures ($> 10^7$ pc cm^{-6}) and high electron densities ($> 10^4$ cm^{-3}). More than one UC H II region may be found within the same star-forming dark cloud.

The formation of massive stars in molecular clouds is a topic that has received a considerable degree of attention in recent years. Several phenomena have proved extremely useful in the identification and classification of candidate regions (Wood & Churchwell 1989a, hereafter WCa; Menten 1991), such as the discovery by Menten of a strong and widespread masing transition of methanol at 6.669 GHz associated with such regions. Also, the identification of such regions by their far-infrared (FIR) colours from measurements with the *Infrared Astronomical Satellite* (*IRAS*) has proven extremely useful (WCa). This paper presents a survey for the methanol line in a sample of southern sources selected as UC H II regions on the basis of their *IRAS* colours.

2 SELECTION CRITERIA

The UV radiation from a massive young star is responsible for heating the dust in and around the H II region, which then re-radiates the energy with a distribution which approximates a blackbody, with the emission peaking in the FIR at around 100 μm. Thus most of the stellar luminosity is expected to manifest itself in the FIR radiation. Almost all of the sky was observed by *IRAS* at FIR wavelengths, hence examination of *IRAS* data can prove very useful in identifying such regions. With a blackbody curve peaking around 100 μm, the differences between the three *IRAS* bands at 12, 25 and 60 μm would indicate that UC H II regions have extremely reddened colours. WCa utilized this information to identify UC H II regions in the *IRAS* Point Source Catalog (*IRAS* PSC) using the selection criteria of equations (1) and (2) where f_{12}, f_{25} and f_{60} are the 12-, 25- and 60-μm *IRAS* fluxes respectively:

$$\log(f_{25}/f_{12}) > 0.57, \quad (1)$$

$$\log(f_{60}/f_{12}) > 1.3. \quad (2)$$

When applied to the *IRAS* PSC for all sources south of declination 0°, 1899 candidates fit the criteria, including those with upper limits in the *IRAS* fluxes at 12, 25 and 60 μm (sources with upper limits in the 25- and 60-μm *IRAS* bands did not fit the WCa selection criteria). This means that our sample includes some *IRAS* sources that would not have been included by WCa. All candidates considered in this survey fit the criteria of equations (1) and (2).

Table 1. The *IRAS* sources in our data set with no positive methanol identification, and no other defining UC H II characteristics.

00260-7315	05327-0529	08189-3602	10257-4338	13054-6159	15584-5247	16571-4029	17488-1741
00445-1207	05329-0508	08245-4038	10263-5923	13093-6203	16026-5035	16596-4012	17527-2439
00462-7331	05329-0628	08303-4303	10276-5711	13107-6208	16037-5223	16598-4156	17531-2426
00466-7322	05331-0515	08375-4109	10295-5746	13120-5453	16056-5207	16599-4232	17555-2436
00574-7226	05356-6604	08438-4340	10309-5803	13291-6249	16064-5212	17006-4223	17591-2228
01035-7215	05338-0624	08448-4343	10309-5745	13294-6011	16067-5449	17028-4050	18028-2059
01053-1746	05338-0647	08476-4306	10312-6004	13300-6543	16069-4858	17044-4134	18035-2126
01077-7327	05339-6847	08485-4419	10320-5928	13338-6312	16072-5123	17074-4549	18060-1816
01126-7332	05355-6736	08516-3952	10337-5710	13342-6345	16083-5154	17077-3929	18063-1828
01133-7336	05363-0702	08563-4711	10365-5803	13353-6309	16116-4905	17095-3837	18080-1804
01228-7324	05375-0731	08576-4334	10374-5924	13367-6106	16128-5109	17103-3702	18089-1837
04496-6917	05387-0924	09002-4732	10411-5930	13408-6143	16164-4929	17118-3909	18092-1742
04521-6928	05391-0217	09002-4020	10419-5925	13419-6159	16164-4837	17130-3923	18098-1814
04522-6925	05391-0152	09006-4830	10424-5916	13428-6158	16177-5018	17136-3816	18111-1729
04531-6808	05393-6930	09017-4813	10430-5931	14039-6113	16179-4951	17136-3617	18116-1646
04542-6916	05393-0156	09017-4814	10441-5823	14090-6052	16186-5044	17146-3723	18118-1733
04546-6915	05394-0151	09028-4837	10451-5936	14137-6123	16235-2416	17150-3754	18127-1717
04566-6629	05400-0154	09058-4521	10501-5556	14170-6002	16251-4929	17162-3731	18130-1626
04573-6849	05405-6946	09078-4905	10559-5914	14192-4355	16293-2422	17178-3742	18222-1317
04574-6829	05423-7120	09094-4803	10564-5833	14212-6009	16316-1540	17258-3637	18227-1227
04580-6626	05458-6947	09108-4915	10591-6040	14382-6017	16330-4725	17317-2743	18234-1444A
05038-6722	06070-0619	09203-5143	11035-6212	14477-5947	16352-4712	17393-2727	18248-2608
05051-6807	06084-0611	09227-5146	11079-6101	14482-5857	16360-4707	17409-2923	18250-1534
05051-7058	06572-0742	09230-5148	11136-6056	14594-5824	16362-4845	17413-2909	18263-1036
05053-6659	07025-1204	09238-5153	11143-6113	14597-5728	16379-4856	17418-2910	18308-0911
05101-6855A	07061-0414	09448-5243	11220-6142	15015-5720	16396-4429	17419-2907	18310-0806
05136-6925	07167-1757	09563-5743	11225-6156	15061-5806	16410-4529	17420-2902	18314-0720
05173-0555	07207-1435	09566-5607	11262-5239	15145-5946	16421-4532	17422-2841	18342-0655
05196-6941	07278-1826	09572-5636	11297-6337	15290-5546	16450-4517	17422-2911	18360-0537
05202-6655	07284-1511	09575-5640	11303-6211	15335-5552	16452-4504	17424-2852	18385-0512
05214-6532	07288-1518	09578-5649	11354-6154	15384-5348	16475-4609	17430-2900	18420-0512
05219-6943	07298-1919	10002-5636	11426-6301	15404-5345	16489-4318	17431-2846	18451-0332
05221-6749	07333-1838	10019-5712	11513-6403	15405-4945	16492-4349	17432-2855	18491-0207
05221-6800	07334-1842	10031-5632	11583-6247	15487-5303	16494-4330	17433-2921	18595-3712
05228-6643	07358-3243	10049-4011	12015-6305	15502-5302	16506-4512	17433-2841	19590-1249
05270-6851	07395-1437	10049-5657	12072-6227	15507-5359	16510-4347	17433-2828	
05277-6729	07399-1435	10106-6217	12127-6244	15513-6600	16527-4504	17454-1627	
05304-0435	07427-2400	10132-5735	12219-1830	15539-5353	16545-4012	17456-2850	
05320-7106	07502-2618	10140-5707	12331-6134	15544-5246	16547-4247	17462-2845	
05325-6629	08140-3559	10178-5736	12413-6332	15550-5306	16561-4006	17462-1959	
05325-6743	08159-3543	10184-5748	12437-6218	15570-5227	16566-4229	17474-2637	

Various techniques were used to reduce the number of candidates to more manageable proportions, as has been previously described (Walsh et al. 1995). The PMN (Parkes–MIT–NRAO: Griffith & Wright 1993) 4.85-GHz radio continuum survey was used to search for point sources associated with the *IRAS* sources. The FWHM of the PMN survey is 4.2 arcmin so that a single beam may be covering more than one UC H II region or possibly picking up more diffuse emission not associated with an UC H II region, but with a larger H II region. Nevertheless, we are confident that associations with the PMN survey will point towards more likely star-forming regions regardless of the nature of the radio continuum emission. The positions of the *IRAS* sources were also checked through the literature for associations with OH, water or other methanol masers (Norris et al. 1987; Kemball, Gaylard & Nicholson 1988; McCutcheon et al. 1988; te Lintel Hekkert et al. 1988, 1989; Braz et al. 1989, 1990; MacLeod 1991; Menten 1991; Palla et al. 1991; te Lintel Hekkert 1991; MacLeod & Gaylard 1992; Henning et al. 1992; Catarzi, Moscardelli & Panella 1993; Schutte et al. 1993). An association was considered to be established if the *IRAS* position was no more than 1 arcmin away from the published positions of the radio continuum or maser sources, as this is approximately the area covered by the *IRAS* beam. From the initial list of 1899 *IRAS* sources, a total of 535 primary candidates were selected to form the core of our survey. We considered these sources to be extremely likely to be associated with UC H II regions, and wished to determine the frequency of methanol maser emission in these candidates.

3 OBSERVATIONS

Methanol maser emission at 6.669 GHz is an excellent indicator of the presence of a very young massive star. The Parkes 64-m radio telescope was used to search for methanol emission in those primary candidates for which no previous data existed. A significant proportion of the *IRAS* sources in the list had previously been identified by Caswell et al. (1995a) also using the Parkes radio telescope. These were not re-observed. However, other previously identified sources, which had been measured using other telescopes, were observed. This ensured that a full data set of the candidates was obtained using the Parkes dish, and under similar observing conditions.

Details of the observations have previously been reported (Walsh et al. 1995). In summary, the observations were made by observing on-source for 5 min and then off-source for 5 min for sky subtraction. The data were reduced using the SPC data reduction package and the resulting spectra covered a velocity range of -130 to 130 km s^{-1}, with a velocity resolution of 0.18 km s^{-1}. This was achieved by taking two spectra for most candidates, with central velocities at 40 and -40 km s^{-1}. Thus, the first spectrum covered the velocity range from -50 to 130 km s^{-1} and the second covered velocities between -130 and 50 km s^{-1}. The 3σ detection limit varies from source to source but is always better than or equal to 1 Jy, and nothing below 0.3 Jy was considered to be due to maser emission. The FWHM of the beam is 3.3 arcmin.

4 RESULTS

As described above, 535 *IRAS* sources have been observed with the Parkes radio telescope to search for the presence of methanol maser emission. The observations were made either as a part of the current programme or by Caswell et al. (1995a). In Table 1, those sources with no detection of methanol emission, and with no previous identification as an UC H II region from continuum emission, are listed. From the 535 *IRAS* sources, 199 have been found to display methanol maser emission, down to the survey limit. We conclude that these 199 *IRAS* sources can be confirmed as UC H II regions. A further two maser sources are included in the beam of IRAS 16513-4316A, and are also considered to be associated with individual UC H II regions.

There are also a total of 36 UC H II regions that have been previously identified by the presence of a compact radio continuum source (Wood & Churchwell 1989b; Kurtz, Churchwell & Wood 1994). Of these, 14 do not exhibit any methanol emission above our detection limits. Therefore there are a total of 215 sources that we can confidently identify as UC H II regions from our list of primary candidates, i.e. about 40 per cent.

In Fig. 1 we present methanol spectra for those maser emission sources that were previously undetected, or for which preliminary results were reported in Walsh et al. (1995). Also included in Fig. 1 is IRAS 17258-3637, which exhibits strong enhanced absorption. Since this survey did not determine positions for the methanol emission, using the *IRAS* positions for pointing the telescope, it is possible that some line intensities are underestimated due to the beam being offset from the emission peak, or even in some cases due to a sidelobe response from a nearby strong source. A few sources do show unrelated FIR radiation and methanol emission (see Section 4.2), but otherwise we do not expect many chance alignments of *IRAS* and methanol sources. A programme is now underway with the Australia Telescope Compact Array to determine accurate positions for both the masing emission and associated radio continuum sources (Walsh et al., in preparation).

Of those *IRAS* sources found to be associated with methanol emission, it is noted that the methanol spectra exhibit a wide range of characteristics. Peak flux densities range from 0.3 to 5090 Jy; the number of individual peaks (maser spots) in any spectrum ranges from 1 to 18, and each spot has a velocity width smaller than that of the velocity resolution of the instrument (0.18 km s^{-1}). Any broadening of a maser peak beyond this resolution is usually attributed to the superposition of two maser peaks that are close in velocity, rather than the broadening of a single maser spot profile.

The number of maser spots cannot be determined absolutely due to the intrinsic detection limit, and any analysis that compares the number of peaks must take this into account. Nevertheless, we can examine the results qualitatively to get an idea of a typical maser emission source. For the 201 maser sources in our survey, the median value for the peak emission is 13 Jy, and there is a median of five maser spots for each spectrum.

The nature of the remaining 322 sources with no detectable methanol emission, nor defining radio continuum for identification with UC H II regions, is still not firmly established. Since they all meet the criteria of equations (1) and (2), it is expected that the great majority are UC H II regions, but further observations are needed to confirm this. The consequences of only 40 per cent of the sample exhibiting methanol emission will be discussed further in Section 5.1.

The results of the maser survey are summarized in Table 2. The first column lists the *IRAS* PSC name; the Galactic longitude and latitude are given in columns 2 and 3, respectively. Columns 4, 5, 6 and 7 show the methanol maser peak flux density, the peak radial velocity, the radial velocity range covered by the methanol emission and the number of maser spots observed above the stated detection limits, respectively. The table indicates the date of observation for the information provided in columns 4 to 7, which is important due to the known variability of some of the masers. Sources such as 17559-2420, where no methanol information is given, do not exhibit any methanol features that were detected, but are included here as they have previously been identified as UC H II regions from their radio continuum emission. Column 8 lists adopted distances to each source, where possible. The kinematic distances are derived assuming that $R_0 = 10$ kpc and $\Theta_0 = 250$ km s^{-1} are the galactocentric distance and rotational velocity, respectively, of the Sun. Some of the sources have two values calculated which is a result of the near–far kinematic distance ambiguity. Other sources have no distance listed (shown as 'ind') due to there being no radial velocity information or because the errors associated with the kinematic distance determinations are too large. Columns 9 and 10 of Table 2 list the calculated luminosity and spectral type of a single star producing the FIR radiation as observed by *IRAS* (see Section 4.1 for an explanation of the method used to determine these values). The two numbers given in some cases correspond to the near and far kinematic distances used. The last column (11) of Table 2 lists associations of each source with other masers or UC H II identifications given in the literature.

4.1 *IRAS* luminosities

Equation (3) can be used to find the luminosity for each source given the four *IRAS* fluxes:

$$F_{\rm tot} = (f_{12}\Delta\nu_{12} + f_{25}\Delta\nu_{25} + f_{60}\Delta\nu_{60} + f_{100}\Delta\nu_{100})/Y, \quad (3)$$

where $F_{\rm tot}$ is the total flux used to derive the values in column 9 of Table 2, f_x is the flux at wavelength x, $\Delta\nu_x$ is the bandwidth at wavelength x and Y is a factor incorporating the flux from the source that is longward of the 100-μm *IRAS* band. For our calculations the values of $\Delta\nu_x$ were taken to be 15 900, 5630, 2920 and 939 GHz for $x = 12$, 25, 60 and 100 μm, respectively (*IRAS* 1985). Previously, WCa estimated that approximately half of the total flux was found longward of the 100-μm band, assuming the factor Y equal to 0.5. Observations (Chini et al. 1986) of some of the sources listed in Table 2 at the longer wavelength of 1300 μm allow us to estimate what this contribution should be, and hence determine Y. There are 22 sources that are UC H II regions appearing in Table 2 which also appear in the list of Chini et al. (1986). From these, an average was derived for the value of Y by fitting a simple curve to the data. The average value for Y was 0.61 ± 0.02. Hence, approximately 40 per

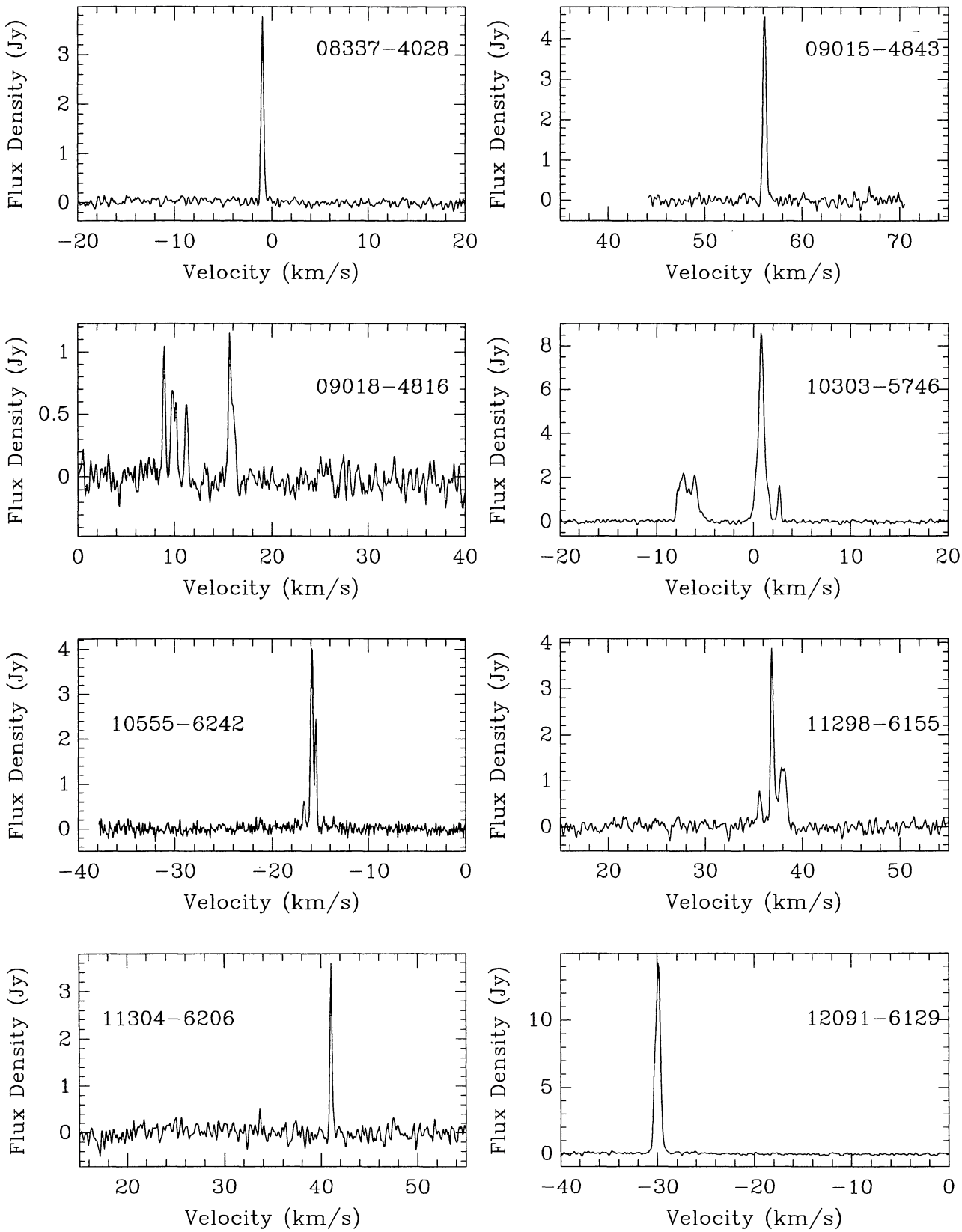

Figure 1. Spectra for those methanol sources discovered in the present work, or published previously by Walsh et al. (1995).

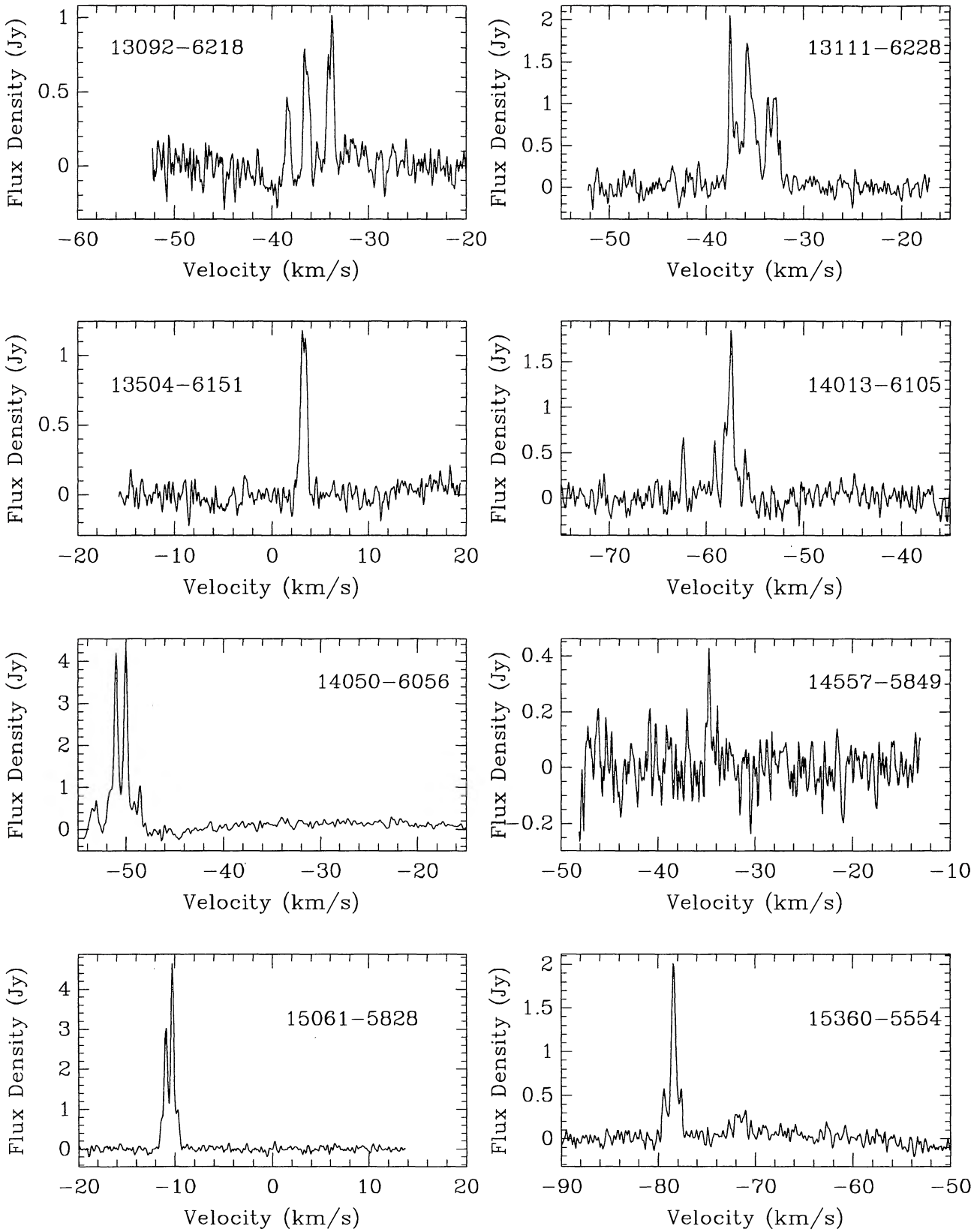

Figure 1 – *continued*

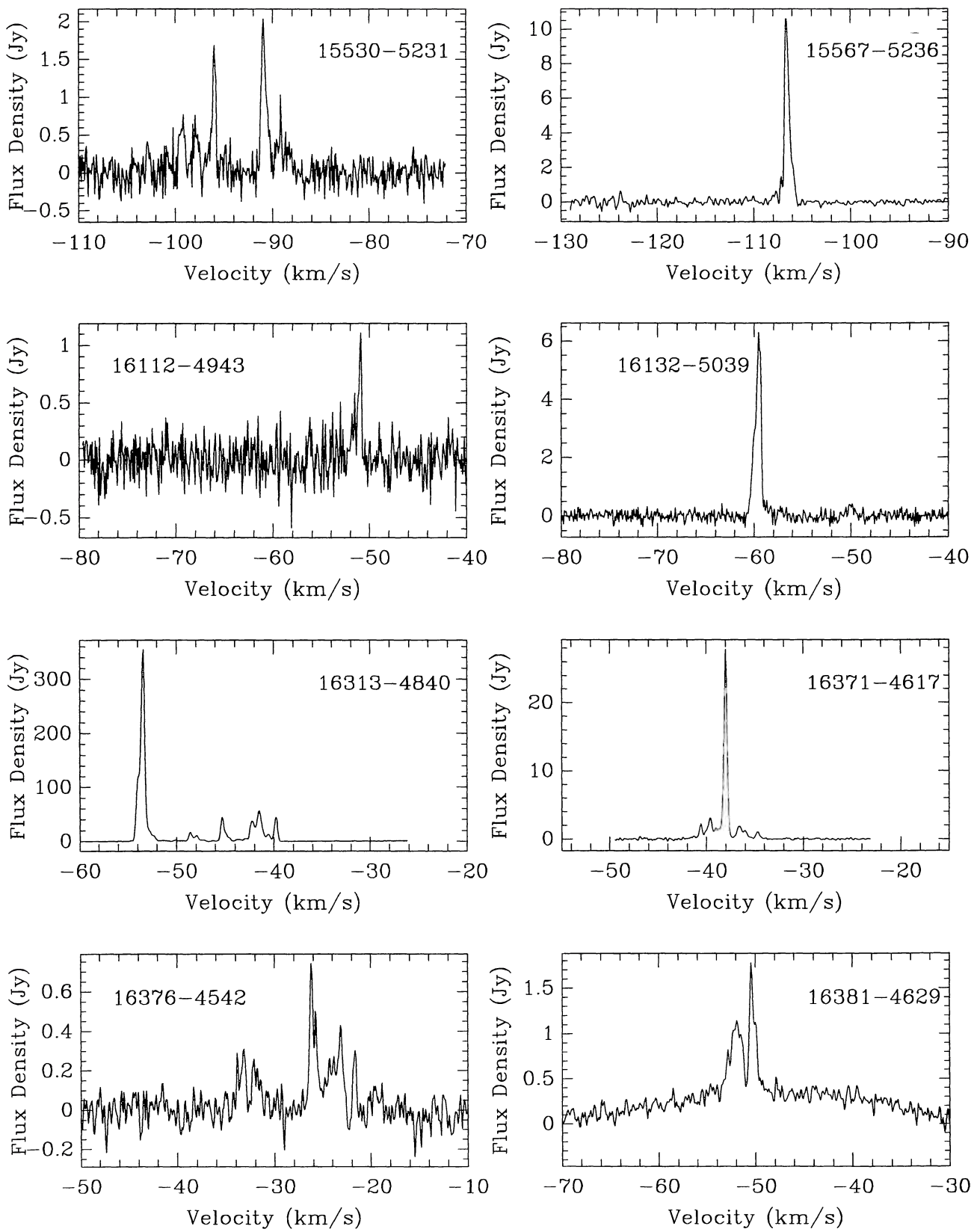

Figure 1 – *continued*

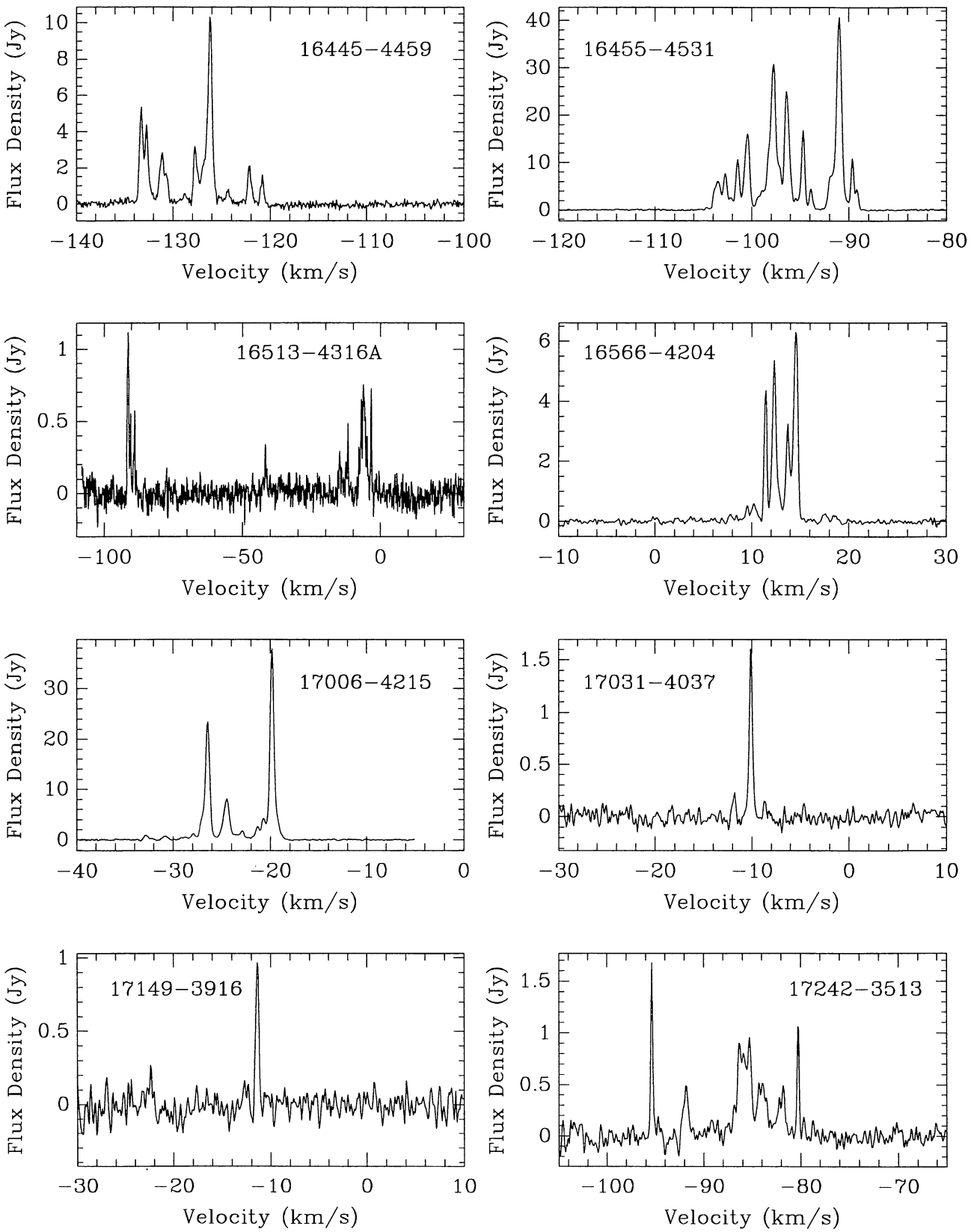

Figure 1 – *continued*

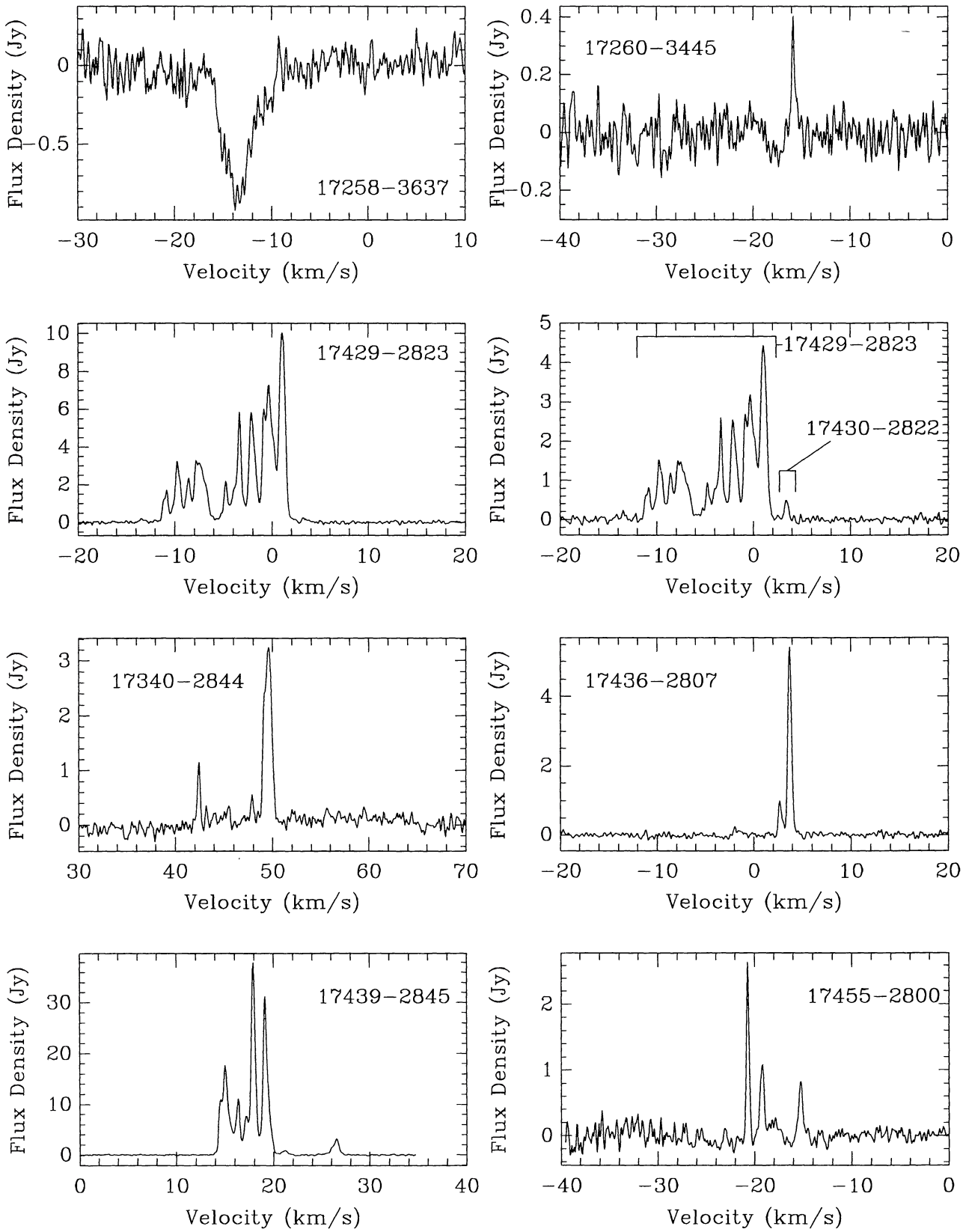

Figure 1 – *continued*

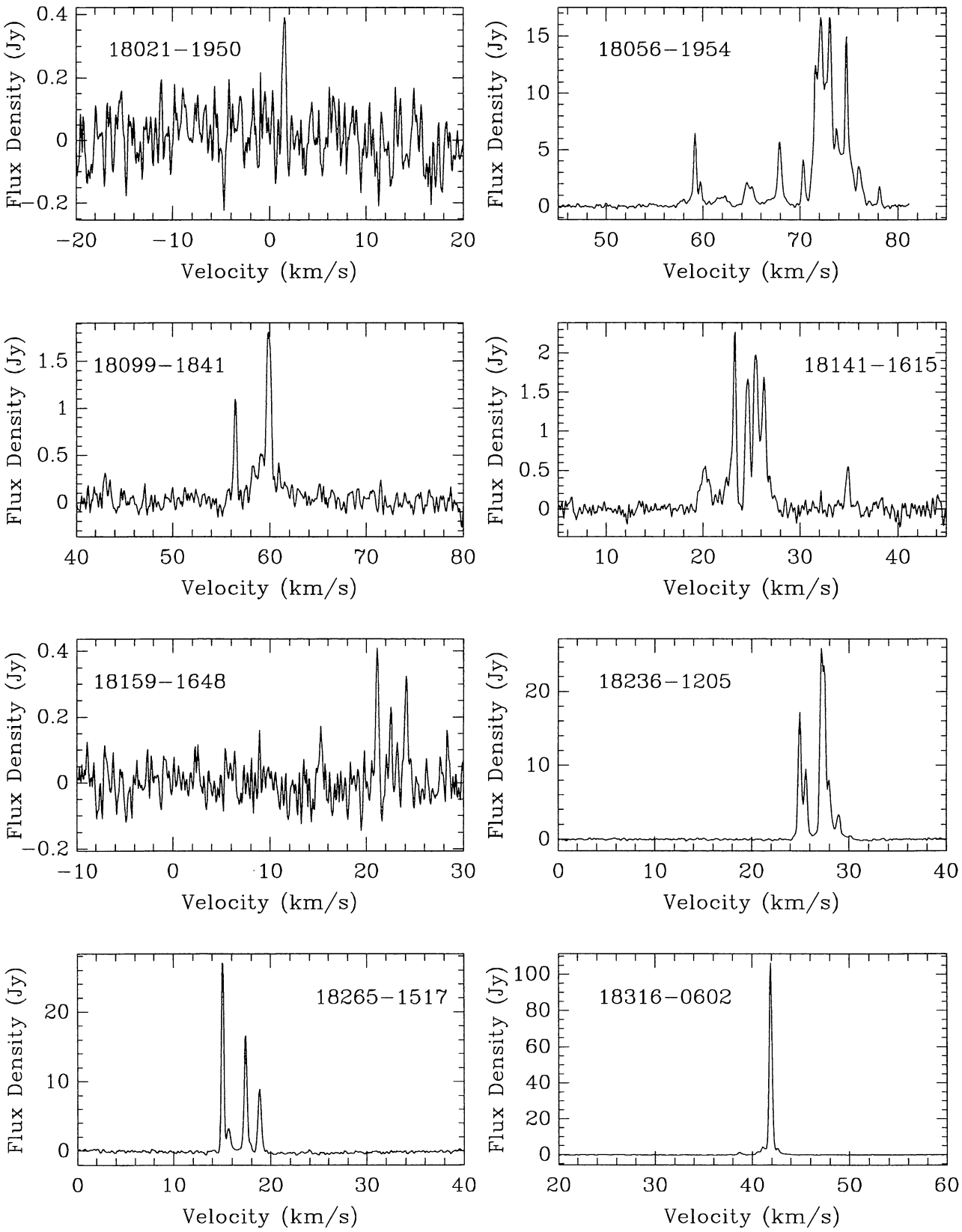

Figure 1 – *continued*

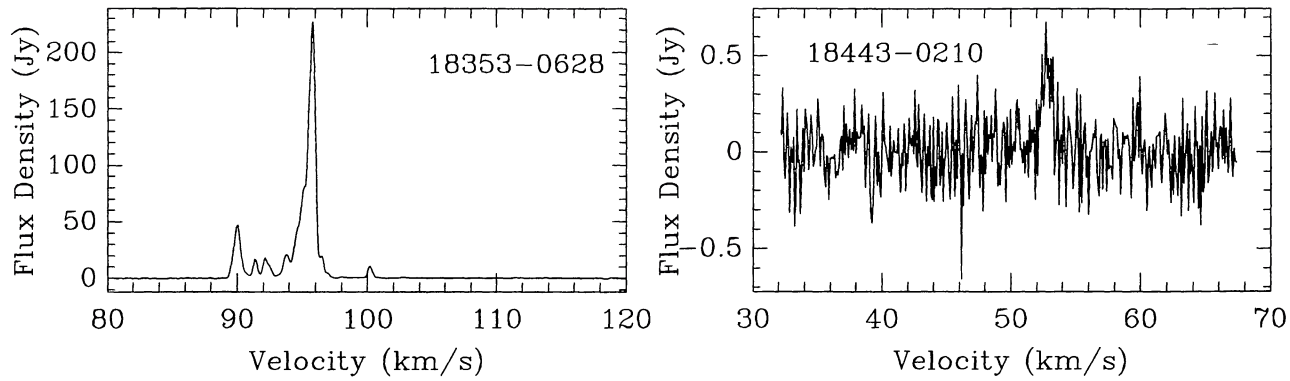

Figure 1 – *continued*

cent of the total flux from the sources is found longward of the *IRAS* 100-μm band.

The value of $Y = 0.6$ was used in equation (3) to calculate the total luminosity for nearly every source listed in Table 2. There are two reasons why some of the sources do not have listed luminosities: the distance could not be determined to the source (as is the case for 08337-4028) or two of the *IRAS* fluxes for the source were upper limits and so an extrapolation to find a total luminosity would be too inaccurate (as is the case for 14567-5846). There are also a number of sources that have one upper limit in their *IRAS* data. For those sources, the other three *IRAS* points were used to determine the luminosity.

The spectral type for each source is obtained directly from the luminosity (Panagia 1973) and is listed in column 10 of Table 2. The assumptions involved in determining the spectral type are: (i) that all the flux of the UC H II region is found between 10 and 1300 μm; (ii) that there is only one star that is responsible for this emission, and (iii) that there is no significant absorption of the infrared radiation by the gas within the region. It has been demonstrated (Kurtz et al. 1994; Wood & Churchwell 1989b) that nearly all the radiation from an UC H II region does indeed appear in the FIR so that there is little reason to doubt the validity of the first assumption. The second assumption that there is only one star responsible for the emission is almost certainly not valid in many cases. The *IRAS* beam is around 1 arcmin in size and so the emission picked up as a point source by *IRAS* may encompass a number of UC H II regions, all forming within the same star-forming region. This is evidenced by the radio continuum maps of Wood & Churchwell (1989b) and Kurtz et al. (1994). It is also evident in sources such as 17441-2822 where the derived luminosity in Table 2 is too large for a single star to be responsible for all the emission. Kurtz et al. (1994) indicate that the assumption of no significant contribution to the luminosity from gas absorption is not true for many cases. Furthermore, since the beam of the Parkes radio telescope at 6.7 GHz is 3.3 arcmin, it is possible that the methanol emission may not be associated with the *IRAS* emission detected, and recent high spatial resolution data (Walsh et al., in preparation) indicates that this is true in a few cases. The purpose of providing spectral types is not to give a definitive classification of each source, but to provide a first-order estimate of the regions based on the *IRAS* data, from which further refinements may be made with more data in the future.

It should also be noted that some of the entries in column 10 of Table 2 indicate two spectral types. This is a result of the ambiguity in the kinematic distance determinations and hence luminosities. It may be possible to use the resultant spectral types to resolve which one of the distances is closer to the true distance, as in some cases one spectral type is clearly unlikely to represent a real object. *IRAS* objects like 15030-5821 can confidently be placed at the far kinematic distance as the near kinematic distance leads to a star that is not luminous enough to produce an UC H II region. There are a considerable number of sources for which the far kinematic distance implies that the single star would be extremely luminous (< O4). It is therefore likely that the near distance can be adopted in these cases. However, since there is the possibility that the luminous emission is due to multiple UC H II regions, the far kinematic distance cannot be completely discounted.

4.2 Notes on individual sources of interest

IRAS 16381-4629. The spectrum obtained by Walsh et al. (1995) and shown in Fig. 1 indicates a peak flux density of around 1.8 Jy. However, Caswell et al. (1995a) obtained a peak flux density of 82 Jy, indicating that the *IRAS* position is offset from the maser source. This is confirmed by recent high-resolution data (Walsh et al., in preparation) which indicate that the methanol source is 6 arcmin to the south-east of the *IRAS* position, casting doubt on the association between the two.

IRAS 16513-4316A. The spectrum for this newly discovered source indicates that more than one system has been detected within the Parkes beam. We therefore have listed each system separately in Table 2. It is not certain that there are three independent systems, as it is impossible to tell with the current data. High-resolution imaging of the region (Walsh et al., in preparation) unfortunately indicates the position of only one of the systems, with peak flux density at $-6\,\mathrm{km\,s^{-1}}$. The system with peak flux density at $-42\,\mathrm{km\,s^{-1}}$ is not apparent and the third system is not covered in velocity with the high-resolution data.

IRAS 17130-3755 and IRAS 17130-3756. The methanol emission detected by Caswell et al. (1995a) lies 1 arcmin from each of the *IRAS* sources, so it is impossible to say with which *IRAS* source (if any) the methanol emission is associated. This is the only case from those sources in Table 2 where the methanol emission may be associated with more than one *IRAS* source.

IRAS 17429-2823 and IRAS 17430-2822. At the position of 17430-2822 we obtain a spectrum essentially identical to that of Schutte et al. (1993). At the position of 17429-2823 we obtain a much stronger source which contains all components except one seen at the position of 17430-2822. We therefore identify the stronger methanol components with 17429-2823 and the component seen only at the position of 17430-2822 with that source, as

Table 2. List of the 215 candidates identified as UC H II regions.

IRAS PSC Name	l^a	b^a	Peak Methanol Flux (Jy)^b	Radial Velocity (km s^{-1})	Velocity Range (km s^{-1})	Maser Spots	Adopted Distance (kpc)^c	Single Star $L_{tot}/10^4$ ($L_\odot$)	Single Star Spectral Type	Other Associations^d
(1)	(2)	(3)	(4)	(5)	(6)	(7)	(8)	(9)	(10)	(11)
05393−0156	206.543	−16.347	–	–	–	–	0.5$^\zeta$	1.1	B0.5	W^e U^f x
06053−0622	213.703	−12.602	200$^\alpha$	12	+10, +13	4	0.8	2.9	B0	W^e U^{gh} M^j
07299−1651	232.621	0.996	180$^\alpha$	23	+21, +24	4	1.4	0.63	B1	O^k W^e M^{jl}
08337−4028	259.941	−0.041	3.8$^\beta$	−2		1	ind			N
08470−4243	263.249	0.514	54$^\alpha$	12	+12, +15	3	1.0	0.28	B2	M^m
08546−4254	264.285	1.465	0.2	9	+6, +10	2	1.5	0.88	B0.5	M^j
09015−4843	269.456	−1.472	4.6$^\alpha$	56		1	6.9	6.7	O8	N
09018−4816	269.159	−1.136	1.1$^\alpha$	16	+8, +17	4	2.7	5.2	O8.5	W^m N M^j
09149−4743	270.247	0.835	1.2	4	+3, +5$^\delta$	1	ind			M^j
10303−5746	285.348	0.002	8.5$^\beta$	+1	−8, +3	4	4.4	2.5	B0	N M^n
10460−5811	287.375	0.645	82	−2	−4, 0	–	3.7	0.36	B2	M^{jn}
10555−6242	290.408	−2.913	4.0$^\beta$	−16	−17, −15	3	3.0	0.58	B1	N
11097−6102	291.277	−0.708	107	−30	−31, −26	3	3.5	58.4	O5	M^j
11101−5829	290.375	1.662	2.4	−24	−28, −22	3	3.0	1.59	B0.5	W^m M^j
11298−6155	293.828	−0.745	3.8$^\alpha$	37	+35, +39	3	10.1	19.4	O6	N
11304−6206	293.950	−0.893	3.6$^\alpha$	41		1	11.1	22.1	O6	N
11332−6258	294.515	−1.622	18	−10	−14, −9	5	1.0/7.1	0.14/6.9	B3/O8	W^m M^{jl}
11368−6312	294.973	−1.730	19$^\alpha$	−13		1	1.4/6.9	0.83/20.2	B0.5/O6	W^m M^m
12091−6129	298.262	0.740	14$^\beta$	−30	−31, −29$^\delta$	1	3.8/5.8	2.2/5.2	B0/O8.5	N
12146−6212	299.015	0.129	8.6	18	+18, +20	2	10.6	9.9	O7	M^j
12272−6240	300.509	−0.179	4.7	7	+5, +11	5	10.5	25.8	O6	M^j
12320−6122	300.969	1.152	5.0$^\alpha$	−37	−40, −36	3	4.9	32.7	O5.5	M^j
12326−6245	301.138	−0.225	1.5	−40	−41, −38	2	4.9	41.0	O5.5	M^j
12405−6238	302.032	−0.062	9$^\beta$	−35	−43, −35	6	3.3/6.9	3.4/14.8	O9.5/O6.5	M^m
13079−6218	305.208	0.206	480	−38	−42, −34	7	4.6/6.9	20.9/47.0	O6/O5.5	M^{jp} O^p
13080−6229	305.202	0.019	52	−33	−44, −29	9	2.8/8.7	13.2/127	O6.5/O4	M^j
13092−6218	305.353	0.198	1$^{\alpha\beta}$	−33	−39, −34	3	3.3/8.1	28.9/174	O6/<O4	N M^j
13111−6228	305.553	0.015	2$^\alpha$	−37	−38, −32	4	3.0/8.7	7.7/64.5	O7.5/O5	N
13134−6242	305.805	−0.246	1.1	−39	−40, −36	2	3.3/8.7	4.2/29.2	O9/O6	M^j
13180−6245	306.326	−0.338	0.3	−24	−25, −22	2	1.9/10.0	0.45/12.5	B1/O6.5	M^j
13471−6120	309.921	0.479	780	−60	−65, −53	9	6.3	42.8	O5.5	M^{jp} O^{pq}
13504−6151	310.179	−0.118	1.2$^\alpha$	3		1	13.0	15.9	O6.5	N
14013−6105	311.625	0.290	1.9$^\alpha$	−58	−63, −56	4	5.0/8.1	16.1/42.2	O6.5/O5.5	N
14030−6144	311.645	−0.381	15	32	+31, +36	3	15.7	33.9	O5.5	M^{jl}
14050−6056	312.109	0.309	4$^\alpha$	−50	−54, −48	5	4.0/9.5	8.6/48.4	O7.5/O5.5	N
14095−6102	312.599	0.043	14	−68	−69, −59	3	6.7	10.1	O7	M^{jl}
14159−6038	313.471	0.190	17	−10	−16, −3	13	0.7/13.2	0.12/43.3	B3/O5.5	M^{jl}
14212−6131	313.763	−0.862	40$^\beta$	−54	−57, −40	11	3.8/10.1	1.5/10.9	B0.5/O7	M^m O^q
14222−6026	314.255	0.105	0.4$^\beta$	−44		1	3.3/10.8	1.4/14.8	B0.5/O6.5	M^m
14394−6004	316.361	−0.363	96	4	+1, +8	10	14.7	45.0	O5.5	W^m M^{jm}
14404−5942	316.643	−0.091	128	−20	−25, −14	9	1.4/13.1	0.27/23.7	B2/O6	M^{jq} O^q
14416−5937	316.814	−0.058	12	−46	−49, −37	6	3.3/11.6	23.8/294	O6/<O4	M^{jl}
14498−5856	318.051	0.085	4	−52	−59, −46	5	4.3/11.1	5.8/38.5	O8.5/O5.5	M^j
14551−6016	318.047	−1.405	7.5	46	+44, +47	–	18.2	10.5	O7	M^j
14557−5849	318.777	−0.151	0.4$^{\alpha\beta}$	−34		1	2.4/12.8	0.82/23.2	B0.5/O6	N
14567−5846	318.948	−0.196	780	−35	−39, −31	11	2.4/12.8			M^{jr}
15030−5821	319.836	−0.200	0.4	−9	−14, −9	2	0.6/15.6	0.019/12.8	>B3/O6.5	M^j
15061−5828	320.124	−0.501	4.6$^\alpha$	−11	−12, −9	3	0.8/17.1	0.096/44.1	B3/O5.5	N
15061−5814	320.234	−0.286	28	−62	−71, −58	10	4.5/10.8	14.6/84.0	O6.5/O5	M^{jl}
15100−5613	321.709	1.167	1.4	−44	−45, −38	3	3.4/12.5	5.0/68.2	O8.5/O5	M^j
15122−5801	321.057	−0.520	27$^{\beta\gamma}$	−62	−69, −54	11	4.4/10.8	9.1/54.7	O7.5/O5	M^m
15254−5621	323.462	−0.080	22	−67	−69, −66	2	4.9/11.1	21.2/109	O6/O4	M^{jr}
15278−5620	323.740	−0.263	2860	−51	−59, −46	15	3.6/12.8	6.9/86.7	O8/O5	M^{jpr} O^p
15360−5554	324.922	−0.564	2.0$^{\alpha\beta}$	−79	−80, −78	2	5.8/10.5	6.5/21.3	O8/O6	N
15408−5356	326.655	0.592	11$^{\beta\gamma}$	−43	−45, −37	3	3.1/13.4	29.3/548	O6/<O4	M^m
15437−5343	327.122	0.508	90	−87	−92, −83	5	6.3/10.2	9.8/25.8	O7/O6	M^{jl}
15454−5335	327.403	0.442	93	−83	−85, −72	12	5.9/10.9	11.5/39.2	O7/O5.5	M^j
15520−5234	328.809	0.633	380	−44	−47, −42	6	3.2/13.6	26.9/486	O6/<O4	M^{jpq} O^{pq}
15530−5231	328.955	0.568	2.1$^{\alpha\beta}$	−91	−100, −88	5	6.8/10.3	15.4/35.40	O6.5/O5.5	N
15541−5349	328.254	−0.533	430	−37	−50, −36	5	2.7/14.2	6.0/166	O8/<O4	M^{jp} O^p
15557−5215	329.457	0.506	10$^{\beta\gamma}$	−72	−74, −60	6	5.1/12.0	2.9/16.0	B0/O6.5	M^m

Table 2 – *continued*

IRAS PSC Name	l^a	b^a	Peak Methanol Flux (Jy)^b	Radial Velocity (km s^{-1})	Velocity Range (km s^{-1})	Maser Spots	Adopted Distance (kpc)^c	Single Star $L_{tot}/10^4$ ($L_\odot$)	Single Star Spectral Type	Other Associations^d
(1)	(2)	(3)	(4)	(5)	(6)	(7)	(8)	(9)	(10)	(11)
15567−5236	329.337	0.147	10.5$^{\alpha}$	−106	−107, −105	2	7.8/9.6	123/186	O4/<O4	N M^s
15596−5301	329.404	−0.458	175$^{\alpha}$	−67	−73, −63	10	4.8/12.9	7.2/51.8	O8/O5.5	M^{jl}
16060−5146	330.954	−0.185	7	−88	−91, −87	4	6.3/11.0	104/317	O4/<O4	M^j
16065−5158	330.877	−0.381	0.8	−73	−73, −56	5	5.1/12.2	48.4/277	O5.5/<O4	M^j
16071−5142	331.133	−0.242	28	−91	−92, −81	7	6.6/10.8	12.1/32.4	O6.5/O5.5	M^j
16076−5134	331.278	−0.188	207	−78	−88, −77	12	5.6/11.9	25.7/117	O6/O4	M^{jp} O^p
16085−5138	331.342	−0.345	92	−65	−73, −61	5	4.7/13.0	15.5/119	O6.5/O4	M^{jl}
16086−5119	331.558	−0.124	47	−104	−105, −94	7	7.8/9.6	93.8/142	05/O4	M^j
16112−4943	332.962	0.773	1.1$^{\alpha\beta}$	−51		1	3.8/13.7	8.9/116	O7.5/O4	N
16132−5039	332.541	−0.128	6.3$^{\alpha\beta}$	−60	−61, −58$^{\delta}$	1	4.4/13.1	13.5/120	O6.5/O4	N
16158−5055	332.652	−0.619	7.1	−50	−52, −50$^{\delta}$	1	3.8/14.0	24.6/333	O6/<O4	M^j
16159−5012	333.161	−0.099	6.3	−95	−96, −91	3	6.8/11.2	14.7/40.0	O6.5/O5.5	M^j
16172−5028	333.122	−0.432	15	−49	−57, −45	3	3.7/13.9	51.7/730	O5.5/<O4	M^j
16175−5002	333.467	−0.166	70	−42	−49, −36	12	3.3/14.6	4.0/77.7	O9.5/O5	M^{jp} O^p
16272−4837	335.587	−0.290	110	−47	−56, −44	12	3.8/14.6	3.1/45.1	O9.5/O5.5	M^{jp} O^p
16297−4757	336.360	−0.140	21	−74	−81, −70	10	5.4/13.0	14.5/84.3	O6.5/O5	M^j
16306−4758	336.433	−0.262	46	−93	−95, −86	8	6.9/11.7			M^j
16313−4729	336.859	−0.006	34	−76	−82, −68	8	5.7/12.8	28.4/143	O6/O4	M^j
16313−4840	336.022	−0.819	350$^{\alpha\beta}$	−54	−55, −39	18	3.8/14.5	4.9/70.6	O9/O5	N M^n
16318−4724	336.993	−0.026	38	−126	−127, −116	9	9.3	51.1	O5.5	M^j
16344−4658	337.615	−0.060	21	−42	−54, −38	13	3.6/15.0	3.6/62.6	O9.5/O5	M^j
16348−4654	337.706	−0.055	145	−55	−58, −43	10	4.5/14.0	4.1/39.9	O9.5/O5.5	M^{jpq} O^{pq}
16351−4722	337.406	−0.405	67	−40	−43, −36	7	3.6/15.0	13.5/234	O6.5/<O4	M^j
16359−4635	338.075	0.015	18	−53	−54, −30	14	4.4/14.2	8.7/90.9	O7.5/O5	M^j
16371−4617	338.438	0.057	28$^{\alpha}$	−38	−42, −34	6	3.3/15.2	4.0/84.0	O9.5/O5	N M^n
16374−4701	337.919	−0.457	47	−38	−41, −36	6	3.3/15.2	42.9/909	O5.5/<O4	M^j
16376−4542	338.926	0.386	0.68$^{\beta}$	−26	−34, −22	4	2.3/16.3			N
16381−4629	338.462	−0.246	83	−50	−57, −49	8	4.3/14.2	5.7/61.6	O8.5/O5	N M^j
16424−4531	339.620	−0.118	83	−36	−39, −30	10	3.3/15.5	2.6/57.7	B0/O5	M^j
16445−4459	340.253	−0.051	10$^{\beta}$	−127	−134, −120	10	9.7	25.9	O6	N
16445−4516	340.054	−0.241	42	−60	−63, −46	6	5.0/13.7	31.6/237	O6/<O4	M^j O^t W^t
16455−4531	339.972	−0.531	40$^{\beta}$	−91	−105, −88	17	7.2/11.7	10.4/27.5	O7/O6	N
16474−4610	339.678	−1.206	70	−21	−41, −21	8	2.0/16.6	0.92/63.5	B0.5/O5	M^{jpl} O^{pt} W^t
16484−4603	339.884	−1.259	1820	−39	−45, −27	12	3.6/15.2	11.1/198	O7/<O4	M^{jp} O^{pt} W^t
16513−4316A	342.363	0.103	1.1$^{\beta}$	−91	−92, −88	3	7.0/12.0	8.0/23.4	O7.5/O6	N
16513−4316A	342.363	0.103	0.4$^{\beta}$	−42		1	3.6/15.0	2.1/36.7	B0/O5.5	N
16513−4316A	342.363	0.103	0.7$^{\beta}$	−6	−16, −2	4	1.3/19.2	1.7/369	B0.5/<O4	N
16533−4009	345.010	1.792	508	−18	−24, −15	11	2.5/17.0	11.8/547	O6.5/<O4	M^{jpq} O^{pqt} W^t
16566−4204	343.911	0.113	11	14	+7, +19	6	21.2	30.8	O6	N M^j
16586−4142	344.422	0.047	16	−71	−73, −63	5	6.3/12.8	42.0/173	O5.5/<O4	M^j
16594−4137	344.582	−0.022	3.4	1	−5, +2	2	19.8	65.6	O5	M^j O^t W^t
17006−4215	344.227	−0.568	118	−20	−33, −16	10	2.7/16.6	4.9/185	O9/<O4	N M^{jp} O^{pt}
17008−4040	345.505	0.346	174	−18	−23, −11	11	2.3/17.1	5.4/297	O8.5/<O4	M^{jp} O^{pt} W^t
17016−4124	345.001	−0.220	448	−22	−32, −20	10	2.7/16.7	7.2/274	O8/<O4	M^{jq} O^q
17031−4037	345.804	0.047	1.6$^{\beta}$	−10	−13, −8	2	1.5/18.0	0.22/31.9	B2/O5.5	N
17052−4001	346.520	0.085	1.8	6		1	20.4	88.1	O5	M^j
17059−4132	345.410	−0.953	2.8	−15	−19, −13	2	1.9/17.3	17.3/1440	O6.5/<O4	M^j O^t W^t
17079−3905	347.579	0.211	2.7	−103	−104, −95	3	8.2/11.4	79.7/154	O5/O4	M^j
17096−3856	347.905	0.050	5.3	−28	−31, −27	4	3.8/15.7	4.5/77.3	O9/O5	M^j
17130−3756	349.096	0.105	30	−77	−83, −74	7	7.5/12.2			M^j O^{pt} W^t
17136−3816	348.891	−0.187	2	1		1	19.7	59.1	O5	M^j O^{pt} W^t
17143−3700	350.012	0.430	6	−31	−37, −29	3	4.9/14.9	7.0/64.8	O8/O5	M^j O^t W^t
17149−3916	348.236	−0.976	1$^{\alpha\beta}$	−12		1	1.9/17.7	7.0/610	O8/<O4	N
17158−3901	348.548	−0.979	74	−13	−23, −7	16	2.1/17.5	2.3/158	B0/O4	M^{jp} O^{pt}
17160−3707	350.104	0.085	41	−74	−76, −60	9	7.5/12.2	73.3/194	O5/<O4	M^j O^t W^t
17165−3554	351.162	0.696	11	−5	−7, −2	4	ind			M^j O^t W^t
17166−3656	350.333	0.095	12$^{\beta}$	−66	−67, −56	6	7.1/12.6	14.0/44.2	O6.5/O5.5	M^m
17167−3854	348.720	−1.039	90	−8	−9, −6	2	1.2/18.1	5.9/1340	O8/<O4	M^j O^t W^t
17175−3544	351.417	0.645	3300	−10	−12, −7	8	2.2/17.8	15.5/1020	O6.5/<O4	M^j O^t W^t
17233−3606	351.775	−0.537	225	2	−9, +3	4	ind			M^j O^t W^t
17220−3609	351.581	−0.353	63	−95	−100, −87	11	8.6/11.3	38.4/66.3	O5.5/O5	M^{jl} O^{pt} W^t

Table 2 – *continued*

IRAS PSC Name	l^a	b^a	Peak Methanol Flux (Jy)^b	Radial Velocity (km s^{-1})	Velocity Range (km s^{-1})	Maser Spots	Adopted Distance (kpc)^c	Single Star $L_{tot}/10^4$ ($L_\odot$)	Single Star Spectral Type	Other Associations^d
(1)	(2)	(3)	(4)	(5)	(6)	(7)	(8)	(9)	(10)	(11)
17234−3405	353.464	0.561	13	−50	−53, −50	3	7.1/12.9	2.6/8.6	B0/O7.5	M^j O^t W^t
17238−3516	352.518	−0.157	6.3	−51	−54, −49	4	7.0/12.8	8.4/28.0	O7.5/O6	M^j O^t W^t
17242−3513	352.602	−0.183	1.7$^\alpha$	−96	−96, −80	7	8.5/11.5	39.6/72.5	O5.5/O5	N
17260−3445	353.216	−0.239	0.4$^\beta$	−16		1	3.7/16.3	2.7/52.8	B0/O5.5	N
17269−3312	354.615	0.473	216	−23	−27, −13	12	5.6/15.0	9.7/69.9	O7/O5	M^{jp} O^p
17271−3439	353.410	−0.360	90	−20	−23, −19	6	4.5/15.6	38.6/464	O5.5/<O4	M^{jpq} U^g O^{pqt}
17278−3541	352.630	−1.067	180$^\beta$	−3	−7, 7	7	ind			M^m
17279−3311	354.722	0.303	18$^\beta$	94	+92, +103	4	8.8	19.4	O6	M^m O^t W^t
17302−3245	355.343	0.148	9.6	20	+5, +21	5	24.4	71.7	O5	M^j U^g O^t W^t
17352−3153	356.660	−0.265	9	−54	−57, −45	6	8.9/11.3	10.2/16.5	O7/O6.5	M^j
17402−2938	359.137	0.030	17	−4	−7, 0	7	ind			M^j O^t W^t
17403−3032	358.381	−0.476	21$^\beta$	2	−6, 13	7	ind			M^m
17429−2823	0.495	0.183	10$^\beta$	1	−11, +2	10	ind			N M^m
17430−2822	0.527	0.182	0.4$^\beta$	3		1	ind			N
17430−2844	0.220	−0.009	3.2$^\beta$	50	+42, +50	3	9.9	52.3	O5.5	N
17432−2835	0.375	0.039	0.7	37	+35, +40	2	10.0	38.8	O5.5	M^j O^t W^t
17436−2807	0.812	0.178	5.4$^\beta$	4	+2, +5	2	ind			N M^n
17439−2845	0.314	−0.199	38$^\alpha$	18	+14, +27	8	ind			N M^n
17440−2823	0.644	−0.043	69	49	+48, +53	–	9.5			M^j
17441−2822	0.666	−0.031	18	70.4	+70, +73	–	9.8	513	<O4	M^j U^g
17441−2910	359.970	−0.460	1	23	+20, +23	2	9.8	51.7	O5.5	M^j O^t W^t
17443−2821	0.692	−0.039	32	68.6	+64, +72	–	9.6			M^j
17455−2800	1.127	−0.107	2.6$^\alpha$	−21	−21, −15	3	10.0	86.2	O5	N
17470−2853	0.548	−0.853	68	14	+8, +20	13	9.1	133	O4	M^j O^{pt} W^t
17480−2636	2.613	0.134	52$^\beta$	3	+2, +20	10	ind			M^m
17559−2420	5.477	−0.243	–	–	–	–	14.3^e	70.5	O5	U^{gh} x
17574−2403	5.898	−0.429	8	10	−1, +13	6	2.6^e	27.6	O6	U^{ghu} M^j O^t W^t
17577−2320	6.553	−0.095	1.6$^\beta$	13	0, +15	2	16.7^e	120	O4	U^h M^m
17599−2148	8.139	0.228	12$^\beta$	+20	+18, +22$^\delta$	1	4.2^e	17.8	O6.5	M^m U^h
18006−2422	5.981	−1.191	–	–	–	–	1.9^e	8.3	O7.5	U^{gh} x
18021−1950	10.092	0.750	0.4$^\beta$	2		1	0.4/19.3	0.0097/22.5	>B3/O6	U^{gh} N
18032−2137	8.671	−0.354	5.6	39		1	6.2^e	23.6	O6	U^f M^j O^t W^t
18032−2032	9.621	0.195	5090	1	−4, +9	10	ind			M^j U^f O^t W^t
18048−2019	9.994	−0.030	28$^\beta$	47	+40, +52	7	5.9/14.8	2.9/18.0	B0/O6.5	M^m W^v
18056−1952	10.471	0.028	61	75	+58, +77	8	7.3^e	59.1	O5	M^{jpr} U^{hu} O^p
18056−1954	10.444	0.007	16.5$^\alpha$	73	+57, +79	15	7.4/12.2			N M^{jp} O^p
18060−2005	10.313	−0.152	80$^{\beta\gamma}$	11	+2, +21	15	6.0^e	69.7	O5	M^m U^h
18064−2020	10.157	−0.354	–	–	–	–	6.0^e	137	O4	U^h x
18067−1921	11.032	0.062	0.7	20	+15, +21	2	3.1/16.5			M^j O^t W^t
18067−1927	10.962	0.016	18$^\beta$	25		1	3.7/16.0	3.1/57.1	O9.5/O5	M^m
18072−1954	10.632	−0.337	3.4	−8	−13, +1	9	21.6			M^j
18073−2046	9.876	−0.750	–	–	–	–	3.9$^\zeta$	3.9	O9.5	U^f x
18075−1956	10.626	−0.383	3.6	5	−10, +7	6	6.5^e	109	O4	U^{ghu} M^j O^t W^t
18085−1931	11.110	−0.399	–	–	–	–	5.2$^\zeta$	7.6	O7.5	U^f x
18089−1732	12.889	0.490	93	39	+27, +43	8	4.7/14.8	8.1/80.1	O7.5/O5	W^v M^{jr}
18090−1832	12.026	−0.034	82	108	+105, +113	9	8.5/11.1	2.6/4.5	B0/O9	M^j
18094−1840	11.935	−0.148	2.3	48	+45, +49	3	5.7/13.9	1.6/9.3	B0.5/O7	M^j
18097−1825A	12.209	−0.103	15	20	+19, +21	3	16.1^e			U^{gh} M^j O^t W^t
18099−1841	11.992	−0.275	1.8$^\beta$	60	+55, +62	2	6.3/13.2	2.3/14.2	O9.5/O6.5	N
18110−1854	11.936	−0.615	47	32	+30, +44	10	4.2/15.0	11.3/144	O7/O4	U^g M^j
18117−1753	12.906	−0.260	317	39	+35, +47	6	4.7/14.7	16.6/162	O5.5/<O4	M^{jq} O^{pqt} W^t
18134−1942	11.499	−1.485	160$^{\beta\gamma}$	7	+5, +17	11	1.6/18.0	0.57/72.7	B1/O5	M^m W^v
18141−1615	14.606	0.013	2.3$^\alpha$	23	+19, +35	6	3.0/16.3	1.2/36.4	B0.5/O5.5	N
18159−1648	14.332	−0.639	0.4$^\beta$	21	+21, +24	2	2.9/16.4	2.6/84.4	B0/O5	W^v N
18162−2048	10.840	−2.591	–	–	–	–	1.9$^\zeta$	2.6	B0	U^{fg} x
18174−1612	15.033	−0.677	39	21	+21, +24	2	2.1^e			M^{jq} U^{gh} O^{qt}
18182−1433	16.586	−0.052	21	59	+52, +69	10	5.4/13.7	3.1/19.7	O9.5/O6	M^j O^t W^t
18217−1252	18.462	−0.008	23	49	+47, +50	2	4.5/14.6	4.8/50.7	O9/O5.5	M^j
18222−1317	18.146	−0.284	–	–	–	–	5.2$^\zeta$	35.0	O5.5	U^f x
18232−1154	19.485	0.150	19.3	21	+20, +27	3	2.1/16.6	1.4/89.4	B0.5/O5	M^j U^f
18228−1312	18.302	−0.391	–	–	–	–	2.9$^\zeta$	5.4	O8.5	U^f x

Table 2 – *continued*

IRAS PSC Name	l^a	b^a	Peak Methanol Flux (Jy)[b]	Radial Velocity ($km\,s^{-1}$)	Velocity Range ($km\,s^{-1}$)	Maser Spots	Adopted Distance (kpc)[c]	Single Star $L_{tot}/10^4$ ($L_\odot$)	Single Star Spectral Type	Other Associations[d]
(1)	(2)	(3)	(4)	(5)	(6)	(7)	(8)	(9)	(10)	(11)
18236−1205	19.364	−0.024	26^{β}	27	+24, +31	5	2.7/16.1	0.78/27.8	B0.5/O6	W^{v} N
18239−1228	19.071	−0.282	–	–	–	–	5.4^{e}	23.4	O6	U^{h} x
18244−1155	19.612	−0.137	18	57	+50, +61	3	4.6/14.0	5.8/53.5	O8.5/O5.5	M^{j} O^{t}
18248−1158	19.618	−0.227	0.4	36	+36, +43	3	4.5^{e}	24.6	O6	U^{gh} M^{j} O^{t} W^{t}
18253−1130	20.082	−0.136	2.9	44		1	3.9/14.8	5.9/84.3	O8.5/O5	U^{g} M^{j}
18265−1517	16.868	−2.158	27^{β}	15	+15, +19	5	1.9/17.0	0.53/42.6	B1/O5.5	N M^{j}
18282−0951	21.880	0.014	15	21	+17, +22	2	1.9/16.5	0.64/48.0	B1/O5.5	M^{j}
18290−0924	22.359	0.064	13^{β}	80	+77, +88	5	6.0/12.4	4.2/17.8	O9/O6.5	M^{13}
18310−0825	23.457	0.068	$2.3^{\beta\gamma}$	87	+82, +92	5	6.4/12.0	2.8/9.7	B0/O7	M^{m}
18311−0809	23.708	0.169	–	–	–	–	9.0^{e}	37.1	O5.5	U^{h} x
18316−0602	25.647	1.053	105^{β}	42	+38, +43	5	3.3/14.6	3.4/66.4	O9.5/O5	W^{u} M^{14} U^{f}
18317−0845	23.245	−0.240	6^{β}	64	+63, +66	2	5.0/13.2	5.3/36.6	O8.5/O5.5	M^{m}
18317−0757	23.955	0.151	–	–	–	–	6.0^{e}	24.6	O6	U^{h} x
18319−0834	23.437	−0.183	77	103	+94, +113	15	9.0^{e}	75.5	O5	U^{h} M^{j} O^{t} W^{t}
18324−0820	23.700	−0.194	26^{β}	78	+58, +81	6	5.8/12.3	4.4/20.0	O9/O6	M^{m}
18335−0711	24.845	0.091	21	110	$+109, +115^{\delta}$	1	8.0/10.1			M^{j}
18353−0628	25.695	0.028	225^{β}	96	+89, +101	9	14.0^{e}	51.5	O5.5	U^{h} N
18361−0627	25.791	−0.141	$7.4^{\beta\gamma}$	92	+90, +100	6	6.3/11.8	6.8/23.7	O8/O6	M^{m}
18403−0417	28.199	−0.049	3.3	99	+94, +102	4	7.2/10.5	26.2/55.8	O6/O5	M^{j} U^{f}
18411−0338	28.861	0.067	1.1	105		1	8.1/9.4	26.4/35.6	O6/O5.5	M^{j} O^{t} W^{t}
18416−0420	28.295	−0.377	62^{β}	82	+40, +95	7	6.2/11.5	40.2/138	O5.5/O4	M^{m} U^{f}
18421−0348	28.840	−0.232	1.3	100	+99, +104	3	7.4/10.2	12.3/23.4	O6.5/O6	M^{j}
18434−0242	29.955	−0.016	206	96	+95, +102	–	9.0^{e}	194	<O4	M^{j} U^{hu}
18440−0148	30.818	0.273	8	105	+100, +111	4	8.3	5.9	O8	M^{j}
18443−0210	30.536	0.018	$0.6^{\alpha\beta}$	53	$+52, +54^{\delta}$	1	13.8^{e}	47.1	O5.5	U^{h} N
18446−0150	30.862	0.120	$2.4^{\beta\gamma}$	102	+37, +108	6	7.6/9.1	18.2/26.2	O6.5/O6	M^{m}
18449−0115	31.412	0.313	11	104	+90, +108	6	8.5^{e}	23.5	O6	M^{jm} U^{gh}
18450−0200	30.758	−0.049	68	92	+88, +95	5	6.7/10.4			M^{j}
18452−0141	31.067	0.051	$3^{\beta\gamma}$	16	+15, +17	2	1.2/15.6	0.29/49.7	B2/O5.5	M^{m}
18456−0129	31.280	0.060	81	110	+102, +114	8	8.5	27.3	O6	M^{j} U^{f} O^{t} W^{t}
18469−0132	31.396	−0.257	–	–	–	–	–			U^{f} x
18479−0005	32.797	0.191	–	–	–	–	13.0^{ζ}	160	<O4	U^{f} x

[a]Galactic coordinates are shown in degrees and are derived from the *IRAS* (B1950) positions or from Caswell et al. (1995a), where the data of Caswell et al. have been used in columns 4 to 7 (see footnote *b*).

[b]The methanol maser data provided in columns 4 to 7 come from three different observation times. The data denoted by an alpha (α) in column 4 were obtained during the period 1993 September 24–27, those denoted β were obtained during the period 1994 April 8–12 and the remaining data are those published by Caswell et al. (1995a). The data reflect the first observation date listed. The objects denoted by a γ have also been observed by Schutte et al. (1993) and a comparison indicates that our observation position was not accurately centred on the maser emission, since our maser peak flux densities are substantially lower than those of Schutte et al. (1993). Those sources with velocity range marked δ probably have more than one methanol emission peak, due to the broad velocity range, but only one maser spot can be unambiguously identified in the spectrum.

[c]The distances given are determined kinematically, using the methanol maser velocity, except for those sources denoted by either ε or ζ. The distances to the sources labelled with an epsilon (ε) were obtained from table 4 of WCb. The distances labelled with ζ were obtained from table 2 of Kurtz et al. (1994). The distances obtained from previous papers tend to agree approximately with our kinematic distance where the kinematic distance could be measured. Those sources indicated by 'ind' have no distance estimate due to the large uncertainties.

[d]M denotes a previous methanol maser detection, O denotes a previous OH maser detection, W denotes a previous water maser detection, U denotes a previous UC H II identification by a compact radio source, N denotes sources discovered in this paper or reported in Walsh et al. (1995) and x denotes a non-detection in methanol emission by us.

[e]Henning et al. (1992); [f]Kurtz et al. (1994); [g]Churchwell (1990); [h]Wood & Churchwell (1989b); [j]Caswell et al. (1995a); [k]Braz et al. (1990); [l]MacLeod & Gaylard (1992); [m]Schutte et al. (1993); [n]van der Walt, Gaylard & MacLeod (1995); [p]Caswell, Vaile & Forster (1995b); [q]Norris et al. (1987); [r]Kemball et al. (1988); [s]Ellingsen et al. (1996a); [t]Forster & Caswell (1989); [u]Cesaroni et al. (1991); [v]Palla et al. (1991).

shown in Fig. 1. This peak of the latter component lies within the noise of the spectrum of Schutte et al. (1993).

IRAS 18056-1952 and IRAS 18056-1954. The region around these masers seems to be confused since there are at least three individual maser sources, identified by Caswell et al. (1995a) within 5 arcmin of each other. This is further confirmed by differences between our spectrum for 18056-1954 and that of the closest maser source identified by Caswell et al. (1995a), G10.45-0.02 (separated by 1.5 arcmin). High-resolution mapping of the region (Walsh et al., in preparation) shows that there are four individual maser sources, three of which are within 1 arcmin of 18056-1952, the fourth being coincident with G10.45-0.02.

IRAS 18361-0627. The measurement at the position of the *IRAS* source reveals a peak flux density of only 7.5 Jy, suggesting that the

source found by Schutte et al. (1993) was on the edge of the beam. More recent high-resolution data taken with the Australia Telescope (Walsh et al., in preparation) indicate that the methanol peak lies 3 arcmin off the *IRAS* position and casts doubt on the identification.

IRAS 18446-0150. Our data suggest that the maser flux density at the position of 18446-0150 is only about one-twentieth of that determined by Schutte et al. (1993). This suggests that the identification with the *IRAS* source may be in error, and this suggestion is confirmed by more recent high-resolution data from the Australia Telescope (Walsh et al., in preparation) which shows the methanol source displaced from the *IRAS* source by some 3.25 arcmin.

5 DISCUSSION

5.1 Methanol maser emission and massive star formation

Methanol maser emission can be classified into two distinct types, according to the origin of the emission. Methanol masers at frequencies of 9.9, 25, 36, 44, 84.5, 95 and 146 GHz are classified as Type I masers and are generally found offset by distances of order 1 pc from UC H II regions, whereas Type II methanol masers show emission at 6.7, 12.2, 19, 23, 37.7, 38.3 and 38.5 GHz (van der Walt et al. 1995). It is generally believed that the 6.7-GHz methanol maser is closely associated with massive star formation. It is not clear, however, that the Class II methanol masers are associated only with massive star formation. There is no evidence so far that such masers are associated with any other type of astrophysical object. However, since OH masers can exist in the same sources (Caswell et al. 1995b) and have also been detected towards red giants, it might be possible for other classes of object to exhibit methanol maser emission, and thus contaminate our sample. There is currently no conclusive evidence for the existence of Class II methanol emission which is not associated with massive star formation.

However, the objects we have identified with maser emission are almost certainly UC H II regions due to their association with an *IRAS* source, fitting the colour–colour selection criteria of equations (1) and (2). WCa have noted that the possible sources of contamination in their selection criteria can be reduced to close, less massive stars or planetary nebulae. The less massive stars (i.e. those not massive enough to produce an UC H II region) will presumably not be efficient enough to produce any significant methanol masing activity due to the much lower flux of FIR radiation compared with the more massive stars, leaving little FIR radiation to pump the maser. Any contamination by planetary nebulae will come from very close objects since the FIR luminosities are typically 10^2–10^4 times less than those for massive stars, as noted by WCa. This implies that for planetary nebulae to have FIR fluxes strong enough to be detected by *IRAS*, they would have to be closer than about 1 kpc for the brightest planetary nebulae. Any planetary nebula of this proximity would have been previously detected and would have been flagged out in the original *IRAS* selection process. Thus, all known sources of contamination can be eliminated from our list so that we can confidently identify each source in Table 2 with an UC H II region.

The identity of the remaining *IRAS* sources in our list of 535 primary candidates is not so certain, although it is still highly likely they are UC H II regions, due to their *IRAS* colours. Using results of Ellingsen et al. (1996a) and Ellingsen, Norris & McCulloch (1996b), and this paper, we attempt to determine the nature of the 322 sources without methanol emission. Ellingsen et al. (1996a) found that about half of the sites of maser emission had no *IRAS* source that could be identified with the emission up to 1 arcmin away. Furthermore, Ellingsen et al. (1996b) found no evidence for a compact radio continuum source above their detection limits in three out of five sites of methanol maser emission that they mapped.

In this work approximately 40 per cent of *IRAS* sources have no methanol emission above our detection limits, even though their *IRAS* colours indicate that most should be UC H II regions. We therefore put forward the following hypothesis as an explanation of these results as it relates to the evolution of an UC H II region. (i) Methanol maser emission commences during an early phase of pre-main-sequence evolution of massive stars, before they are hot enough or evolved enough to ionize the surrounding gas. This is therefore before they are observable either as a compact radio source or as a bright *IRAS* source. Such a scenario would apply to the methanol sources detected by Ellingsen et al. (1996a,b) discussed above. (ii) The maser emission remains for a large proportion of the ultracompact phase (roughly 40 per cent of the time-scale of the UC H II regions themselves); the majority of sources in Table 2 are expected to be in this phase. (iii) Following this, the UC H II region exists without methanol maser emission. Evidence for this last phase, in which presumably the *IRAS* sources listed in Table 1 are located, is also provided by their broader latitude distribution about the Galactic plane (see Section 5.2 and Fig. 3). Problems still exist with this hypothesis, most particularly the pumping mechanism for the methanol sources in part (i) of this scheme without the associated FIR emission.

5.2 Galactic position

One method of analysis that can be applied to the data is to locate the source positions within the Galaxy, using Galactic coordinates and kinematic distances. The kinematic distances may have large errors associated with them that limit the usefulness of any Galactic plot, but, taking this caution into consideration, it is still possible to obtain some interesting results. The largest errors in the kinematic distances come from the near–far ambiguity in which the velocity and position of an object could indicate that it is on either the near or far side of the Galaxy. To minimize this problem, the literature was referred to where possible, to obtain distance estimates that resolve the ambiguity by employing methods other than using velocities and Galactic longitudes to determine the distance. A further refinement in establishing distances was obtained from the luminosity estimates of some of the sources. If it was obvious that the near kinematic distance would have led to a luminosity far less than that expected for an UC H II region, then the far kinematic distance was used, as in 18021-1950. The near kinematic distance was used for those sources that could not have their distance ambiguity resolved.

Fig. 2 shows a plot of all the methanol sources and UC H II regions from the survey list. There is no clear structure evident in the distribution of the UC H II regions. It is therefore not clear what relationship (if any) there is between the spiral arms of the Galaxy and the UC H II regions. It is interesting to note that the sources are not confined to the spiral arms and there seems to be a large proportion of them lying between the Sagittarius–Carina and Scutum–Crux arms. The main limiting factor on interpretation of the structure of the distribution is that the survey concentrates only on those candidates that are below a declination of 0°. This is unfortunate only in that one of the spiral arms seems to be traced (Scutum–Crux) but is too close to the declination 0° boundary for a confirmation to be made. A larger sample of UC H II regions will be

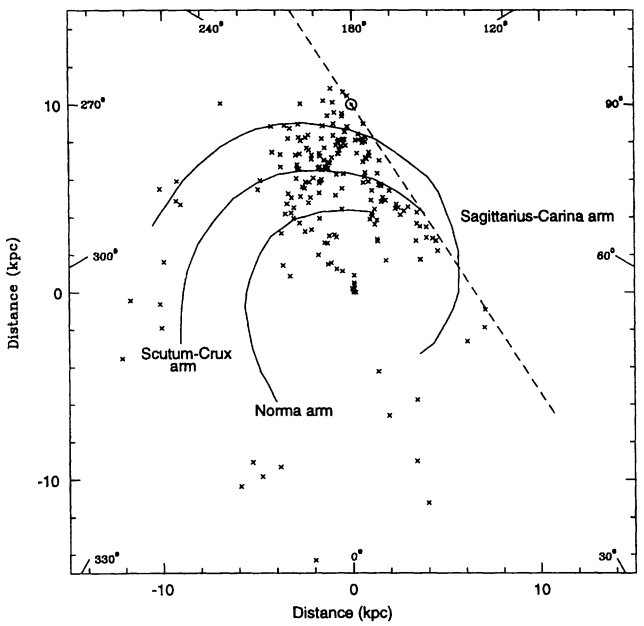

Figure 2. Plot of the identified regions projected from a viewpoint below the Galactic plane. The Galactic Centre is situated at (0, 0) and the Sun is located at (0, 10). The dashed line indicates the limit of our survey, at declination of 0°. The position of the spiral arms is determined using high excitation parameter H II regions (Georgelin & Georgelin 1976).

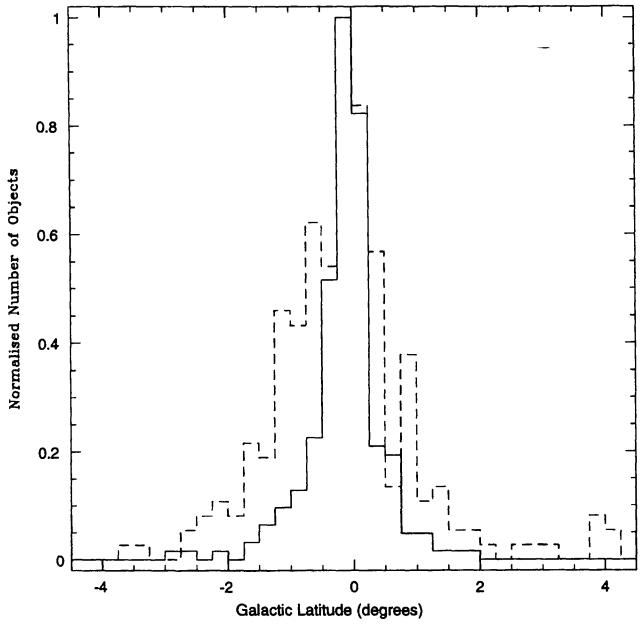

Figure 3. The normalized distribution of the identified UC H II regions with respect to angular distance from the Galactic plane is shown as the solid line. The dashed line represents those sources that do not have methanol emission, or a compact radio continuum source, and so cannot be positively identified with an UC H II region.

more useful in identifying the spiral arms only if the distances to the objects in the sample are determined more accurately than the kinematic distances that have been used here.

A further instructive view of the candidates is shown in Fig. 3 both for identified UC H II regions and for all those sources in Table 1 that were not positively identified as an UC H II region. It shows the number of sources plotted as a function of Galactic latitude. It is obvious that all the candidates are concentrated near the Galactic plane, as pointed out previously by WCa and van der Walt et al. (1995). What is of more importance is the scaleheight of the candidates from the Galactic plane. WCa previously determined a scaleheight of $0\overset{\circ}{.}6 \pm 0\overset{\circ}{.}05$ (corresponding to a FWHM of $0\overset{\circ}{.}8 \pm 0\overset{\circ}{.}06$) for all the sources fitting their criteria. The scaleheight is important to know as it is an indicator of contamination by later type stars (such as early B-type stars) which are presumably not so tightly constrained to the Galactic plane. Contamination may also be the result of extragalactic objects, as well as other sources dealt with by WCa, but not to such an extent as the occurrence of early B stars. It is supposed that early B-type stars are the smallest stars that are luminous and massive enough to produce Lyman continuum photons and hence an UC H II region, so it is debatable whether one would consider such objects as contamination. The results for all our 535 candidates not surprisingly follow the scaleheight of WCa, where our value for the scaleheight is $0\overset{\circ}{.}6 \pm 0\overset{\circ}{.}1$, since these data are similar to WCa's. Fig. 3, though, shows the distribution of massive, embedded YSOs, identified by their methanol emission or UC H II identification as the solid line. This data set is found to be somewhat more closely constrained to the Galactic plane than for all our candidate regions, with a scaleheight of $0\overset{\circ}{.}4 \pm 0\overset{\circ}{.}1$. The implication of this is that the 535 candidates include objects that are not evident in the list of the 215 identified UC H II regions. The remaining 322 which do not show evidence for methanol emission exhibit a broader distribution about the Galactic plane (a scaleheight of $0\overset{\circ}{.}8 \pm 0\overset{\circ}{.}1$) shown by the dotted line. According to our hypothesis in Section 5.1, it is possible that the broader distribution, traced by the dotted line, is a result of older UC H II regions where methanol maser activity has ceased and the sources have had more time to move away from the plane of the Galaxy.

5.3 Maser luminosities and maser spot frequency

As has been previously found (van der Walt et al. 1995), there is little or no correlation between the methanol maser flux density and *IRAS* flux density, other than that there seems to be an upper limit to the peak methanol maser flux density, not exceeding that of the *IRAS* 100-μm flux density. This result is confirmed by our work and is illustrated in Fig. 4 where we have plotted the methanol maser luminosity against the single star luminosity, as shown in column 9 of Table 2. The methanol maser luminosity is calculated from equation (4):

$$L = 4\pi d^2 f \Delta\nu, \tag{4}$$

where L is the maser luminosity, d is the distance to the source (column 8, Table 2), f is the integrated flux density of the maser emission and $\Delta\nu$ is taken to be the FWHM of a single maser spot profile, as measured in the Parkes spectra (11 kHz). Fig. 4 shows that although there is little correlation between the methanol maser and total luminosities, there is apparently an upper limit to the methanol emission with respect to the total luminosity. The dashed line indicates this upper limit, which we can interpret as an upper limit to the efficiency of the pumping mechanism of the methanol maser of approximately 6×10^{-9} of the total luminosity. Since methanol emission is found where there is no FIR emission apparent and there is little correlation between the two, it might lead us to question whether FIR radiation can be the pumping mechanism. Other factors might play an important role in producing the maser emission. We

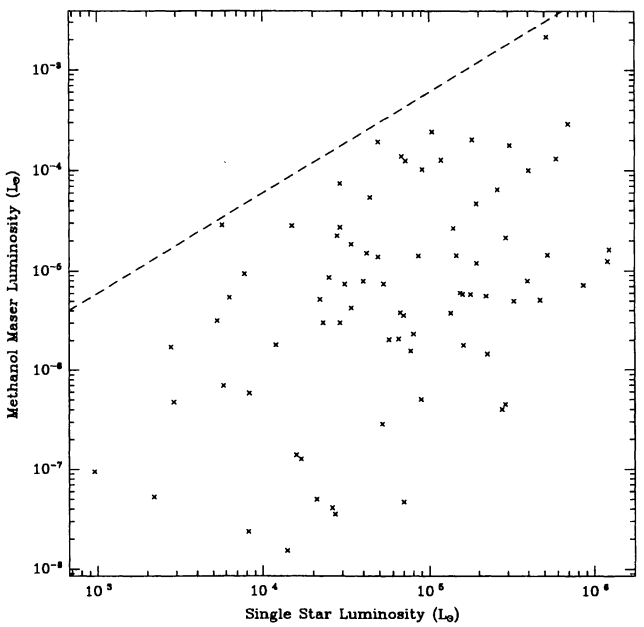

Figure 4. A plot of methanol maser luminosity versus the single star luminosity (Table 2, column 9). The dashed line indicates an upper limit on the maser pumping efficiency, equivalent to 6×10^{-9} of the total luminosity.

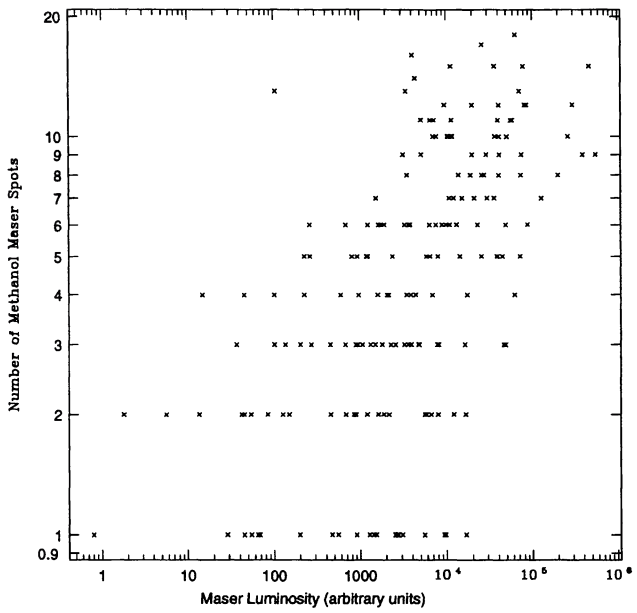

Figure 5. A plot of the number of methanol maser spots against a measure of the methanol peak luminosity.

point out that there are errors that may be obscuring any correlation between the methanol and total luminosities in Fig. 4. The two major sources of errors are the uncertainty in the kinematic distances to the regions, and the fact that the methanol flux density may be underestimated due to offsets in pointing from the site of emission, as described in Section 4. We expect neither of these errors to affect the upper limit seen in the data greatly.

In Fig. 5 we plot the number of methanol maser spots against a measure of the methanol luminosity (determined as the product of the peak maser flux density and the square of the source distance). While there is a 4–5 orders of magnitude range in luminosity between sources for a given spot number, the *maximum* maser luminosity is correlated with the number of maser spots present. We speculate that the abundance of methanol is an important factor in determining the strength of maser emission, and its variation between sources, together with the availability of IR photons for pumping, controls the maser luminosity.

6 CONCLUSIONS AND FURTHER OBSERVATIONS

A survey of UC H II regions has been carried out by searching for 6.669-GHz methanol maser emission from objects chosen from the *IRAS* PSC on the basis of colour–colour selection criteria. Further selections were made by looking for evidence of radio continuum emission, OH, water or methanol maser emission. The resulting 535 candidates have all been observed for methanol emission using the Parkes radio telescope by either us or Caswell et al. (1995a) and the observations provide a standard survey of a large selection of UC H II region candidates. A total of 215 UC H II regions were identified by their methanol maser emission. The positions of the 215 regions within the Galaxy do suggest that there is little evidence for structure and there may be a large number of regions lying between the spiral arms, but the inherent errors in the kinematic distance determinations limit the usefulness of such data. Our data on methanol emission sources associated with UC H II regions show that their Galactic latitude distribution is highly confined to the plane, with a scaleheight of $0\overset{\circ}{.}4 \pm 0\overset{\circ}{.}1$. They thus exhibit a smaller scaleheight than the WCa sample, suggesting that the full WCa sample may include the full range of ages of UC H II regions, whereas those sources with methanol may contain only the younger regions. The methanol emission may be more dependent on the abundance of methanol than on the FIR radiation, as shown by a correlation between the number of methanol maser spots and the peak methanol luminosity and a lack of correlation between the maser luminosity and the total luminosity (governed by the FIR luminosity). A tentative upper limit can be put on the efficiency of the pumping mechanism at 6×10^{-9} of the total luminosity.

This work is being extended to cover near-infrared (NIR) images of selected UC H II regions, as well as high-resolution radio continuum and methanol maser maps. The NIR images will be used to study the nature of the stellar source associated with the UC H II region. The NIR colours will allow us to evaluate the extinction associated with each region, a necessary measurement for establishing the nature of the physical environs. The radio data will be used in conjunction with the NIR and *IRAS* data to pinpoint the UC H II regions within a star-forming cloud and also to examine the morphologies and characteristics of selected regions.

ACKNOWLEDGMENTS

The authors would like to express gratitude to the ATNF for generous allocation of observing time at Parkes, and to J. L. Caswell for helpful discussions on the observing and data reduction. The authors would also like to thank an anonymous referee for valuable comments. Help on early observing runs by Tyler Bourke is also greatly appreciated. This work was partially supported by an Australian Research Council grant. The SPC data reduction package is provided by the ATNF.

REFERENCES

Braz M. A., Scalise E., Jr, Gregorio Hetem J. C., Monteiro do Vale J. L., Gaylard M., 1989, A&AS, 77, 465

Braz M. A., Lépine J. R. D., Sivagnanam P., Le Squeren A. M., 1990, A&A, 236, 479

Caswell J. L., Vaile R. A., Ellingsen S. P., Whiteoak J. B., Norris R. P., 1995a, MNRAS, 272, 96

Caswell J. L., Vaile R. A., Forster J. R., 1995b, MNRAS, 277, 210

Catarzi M., Moscadelli L., Panella D., 1993, A&AS, 98, 127

Cesaroni R., Walmsley C. M., Kömpe C., Churchwell E., 1991, A&A, 252, 278

Chini R., Kreysa E., Mezger P. G., Gemünd H.-P., 1986, A&A, 154, L8

Churchwell E., 1990, A&AR, 2, 79

Ellingsen S. P., von Bibra M. L., McCulloch P. M., Norris R. P., Deshpande A. A., Phillips C. J., 1996a, MNRAS, 280, 378

Ellingsen S. P., Norris R. P., McCulloch P. M., 1996b, MNRAS, 279, 101

Forster J. R., Caswell J. L., 1989, A&A, 213, 339

Georgelin Y. M., Georgelin Y. P., 1976, A&A, 49, 57

Griffith M. R., Wright A. E., 1993, AJ, 105, 1666

Henning T., Cesaroni R., Walmsley M., Pfau W., 1992, A&AS, 93, 525

IRAS Catalogs and Atlases, Explanatory Supplement, 1985, Beichman C. A., Neugebauer G., Habing H. J., Clegg P. E., Chester T. J. eds. GPO, Washington

Kemball A. J., Gaylard M. J., Nicolson G. D., 1988, ApJ, 331, L37

Kurtz S., Churchwell E., Wood D. O. S., 1994, ApJS, 91, 659

te Lintel Hekkert P., 1991, A&A, 248, 209

te Lintel Hekkert P., Habing H. J., Caswell J. L., Norris R. P., Haynes R. F., 1988, A&A, 202, L19

te Lintel Hekkert P., Versteege-Hensel H. A., Habing H. J., Wiertz M., 1989, A&AS, 78, 399

McCutcheon W. H., Wellington K. J., Norris R. P., Caswell J. L., Kesteven M. J., Reynolds J. E., Peng R. S., 1988, ApJ, 333, L79

MacLeod G. C., 1991, MNRAS, 252, 36P

MacLeod G. C., Gaylard M. J., 1992, MNRAS, 256, 519

Menten K. M., 1991, ApJ, 380, L75

Norris R. P., Caswell J. L., Gardner F. F., Wellington K. J., 1987, ApJ, 321, L159

Palla F., Brand J., Cesaroni R., Comoretto G., Felli M., 1991, A&A, 246, 249

Panagia N., 1973, AJ, 78, 929

Schutte A. J., van der Walt D. J., Gaylard M. J., MacLeod G. C., 1993, MNRAS, 261, 783

van der Walt D. J., Gaylard M. J., MacLeod G. C., 1995, A&AS, 110, 81

Walsh A. J., Hyland A. R., Robinson G., Bourke T. L. and James S. D., 1995, Publ. Astron. Soc. Aust., 12, 186

Wood D. O. S., Churchwell E., 1989a, ApJ, 340, 265 (WCa)

Wood D. O. S., Churchwell E., 1989b, ApJS, 69, 831

This paper has been typeset from a TEX/LATEX file prepared by the author.